Maximally Flat Negative Group-Delay Circuit: A Microwave Transversal Filter Approach

Chung-Tse Michael Wu, *Student Member, IEEE*, and Tatsuo Itoh, *Life Fellow, IEEE*

***Abstract*—A comprehensive method to synthesize negative group delay (NGD) in the microwave regime with a maximally flat response is proposed in this paper. This method is based on transversal-filter topologies; it will be shown that by choosing proper coupling coefficients of each tap of a transversal filter, we can realize NGDs with maximally flat characteristics at the output of the transversal filter. The desired coefficients to realize maximally flat NGDs with various amount of group delay are analytically derived and tabulated in this paper. Furthermore, the results are verified experimentally through microwave transversal-filter approaches in both passive and active ways using multi-section asymmetric directional couplers and distributed amplifiers.**

***Index Terms*—Anomalous dispersion, directional couplers, dispersion engineering, distributed amplifiers (DAs), negative group delay (NGD), transversal filters.**

I. Introduction

THE phenomenon of negative group delay (NGD) might yield the output peak of a wave packet preceding the input peak. This is due to the RLC time constants of the circuitry that affect different frequency components of the modulated signal in such a way that some emerge before others when exanimating in the time domain. The emphasis is on the R content of the time constant because without the R, NGD is not exhibited. This, however, does not violate the causality since the initial transient pulse is still limited to the front velocity, which will never exceed the speed of light [1], [2].

In electronic circuits, the NGD phenomenon has exhibited its feasibility using simple low-pass and bandpass amplifiers at low frequency [3]–[5]. Since NGD occurs at the range of frequencies where the absorption or the attenuation is maximum [2], conventionally, in the microwave regime, bandstop structures are used to realize NGD circuitry. Based on either series or shunt RLC resonators, many active and passive NGD circuitries have been proposed and demonstrated with or without tunability [6]–[11].

Very recently, a novel active NGD circuit using distributed amplifiers (DAs) has been proposed [12]. The active NGD circuit is essentially based on the concept of transversal filters [13], [14], which have been typically used in equalization and pulse shaping. By selecting the proper gain coefficients of each tap of the DA by means of convex optimization, the DA is able to synthesize the NGD at its reverse port, while maintaining a flat gain at its forward port as a conventional DA. Furthermore, the NGD-DA is reconfigurable because the amount of NGD can be controlled by changing the gate bias of each device.

Similarly, the concept can also be applied in passive structures by using multi-section asymmetric directional couplers [15]. In this instance, if proper coupling ratios among each coupler are chosen, we can realize NGD at the coupled port of the entire multi-section directional coupler, which results in a fully distributed-element based NGD circuit with no lumped components needed, except the termination 50-Ω loads.

Compared to conventional NGD circuits based on lumped circuits, the aforementioned NGD circuits using transversal-filter topologies can typically achieve a wider bandwidth of NGD (more than 40% relative bandwidth). However, the desired coefficients in previous work were obtained by the convex optimization, a numerical optimization approach, which usually does not give us exact solutions [12], [15]. Therefore, in this paper, we provide a comprehensive method to analytically derive the desired coefficients for transversal-filter-based NGD circuits, which give exact solutions to realize NGD with maximally flat characteristics. Furthermore, the desired coefficients are tabulated for the ease of use. In order to verify the results, passive and active transversal filters based on multi-section directional couplers and DAs are designed and used to examine the NGD responses. The structure of this paper is organized as follows. Section II will analyze a transversal filter from a discrete-time point of view. We will then derive the desired coefficients for maximally flat NGD in Section III. Section IV will illustrate the frequency response of an NGD network. Finally, passive and active realizations of the proposed design method will be illustrated in Sections V and VI, respectively.

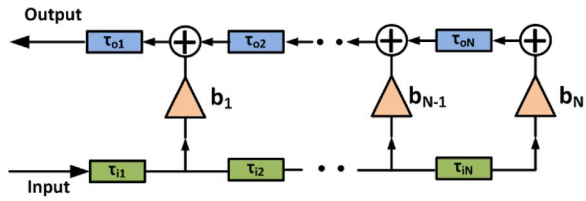

Fig. 1. General diagram of a transversal filter.

II. Transversal-Filter Analysis

Fig. 1 illustrates a general diagram of a continuous time transversal filter. It consists of delay lines (τ), weighting coef-

Manuscript received January 17, 2014; revised April 16, 2014; accepted April 16, 2014. Date of publication April 30, 2014; date of current version June 02, 2014.

The authors are with the Electrical Engineering Department, University of California at Los Angeles (UCLA), Los Angeles, CA 90095 USA (e-mail: michael.wu@ucla.edu).

Color versions of one or more of the figures in this paper are available online at http://ieeexplore.ieee.org.

Digital Object Identifier 10.1109/TMTT.2014.2320220

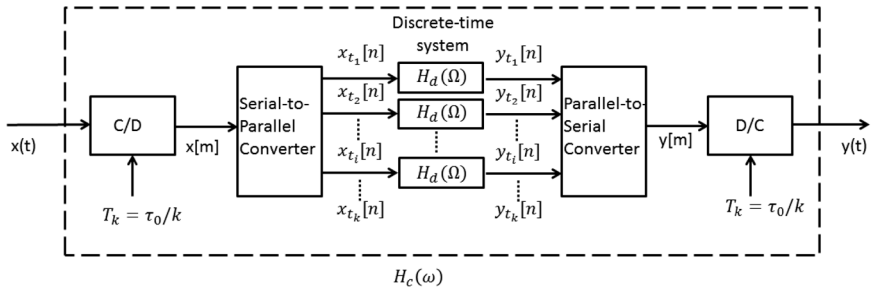

Fig. 2. Equivalent system for a continuous-time transversal filter.

ficients (b_N) and summing operators. The relation of input $x(t)$ and output $y(t)$ in the time domain of a transversal filter with N weighting elements or N sections can be expressed as [13]

$$y(t) = \sum_{n=1}^{N} b_n \cdot x\left(t - \sum_{m=1}^{n} (\tau_{im} + \tau_{om})\right) \tag{1}$$

$$\begin{aligned} Y(\omega) &= X(\omega) \cdot \sum_{n=1}^{N} b_n \cdot e^{-j\omega\left(\sum_{m=1}^{n}(\tau_{im}+\tau_{om})\right)} \\ &= X(\omega) \cdot H_c(\omega) \end{aligned} \tag{2}$$

Its transfer function in the frequency domain can then be obtained by taking the Fourier transform, which is given in (2). Now, if we assume that $\tau_{im} = \tau_{om} = \tau_0$, it follows that the transfer function becomes

$$H_c(\omega) = \sum_{n=1}^{N} b_n \cdot e^{-jn\omega 2\tau_0}. \tag{3}$$

One can notice that (3) has the same mathematical form as that of a discrete-time system. If we denote $\Omega = \omega\tau_0 = \omega T$, then (3) will have the following form:

$$H_d(\Omega) = \sum_{n=1}^{N} b_n \cdot e^{-j2n\Omega}. \tag{4}$$

From (4), we can observe that the continuous-time system described in Fig. 1 is equivalent to a discrete-time system that has a sampling period of $T = \tau_0$[16]. This can be visualized as follows: assuming at certain instantaneous time $t = t_0$, from (1), the output $t(t = t_0)$ is

$$y(t_0) = \sum_{n=1}^{N} b_n \cdot x(t_0 - 2n\tau_0) \tag{5}$$

which means the output only depends on N instantaneous values of the input, i.e., $x(t_0-2\tau_0), x(t_0-4\tau_0)\ldots, x(t_0-2N)$. Since the time domain is continuous, it follows that at any instantaneous time t_i, the system will always generate output based on the previous N instantaneous input values with a time interval of $2\tau_0$. Therefore, the continuous-time transversal filter depicted in Fig. 1 can be considered as infinite numbers of discrete-time transversal filters in parallel with the same sampling period T, but different instantaneous time t_i. The diagram of the equivalent system for a continuous-time transversal filter is illustrated in Fig. 2. When the input $x(t)$ enters the system, it will be sampled with a sampling period of $T_k = \tau_0/k$ through a continuous-to-discrete-time (C/D) converter. It follows that

$$x_{t_i}[n] = x(nT + t_i), \qquad -\infty < n < \infty \tag{6a}$$

$$x[m] = \{x_{t_i}[n] : 1 \le i \le k\}, \qquad m = (n-1)k + i \tag{6b}$$

where $k \to \infty$ since, in reality, there are infinite numbers of instantaneous time t_i. Through a serial-to-parallel converter, $x[m]$, will break down to subsets of $x_{t_i}[n]$. Each discrete-time input $x_{t_i}[n]$ will then enter the discrete-time system whose transfer function is expressed in (4). The discrete-time outputs $y_{t_i}[n]$ generated by each input $x_{t_i}[n]$ are combined together through a parallel-to-serial converter and then all together form an entire output $y(t)$ in the continuous time domain. In other word, the continuous-time transversal filter shown in Fig. 1 will behave like a discrete-time system at any instantaneous time $t = t_i$, and therefore the techniques used in discrete-time signal processing can also be adapted to carry out the analysis.

III. Maximally Flat NGD

With the means of transversal filters mentioned above, we can design NGD circuits operated in microwave bands. Furthermore, our objective is to design the NGD circuits with maximally flat group-delay responses.

A. Derivations of Maximally Flat NGD Responses

From the discussion in Section II, we know that we can use discrete-time transfer function to analyze the transversal filters. The group delay of (4) at $\Omega = \Omega_0$ can be written as

$$\tau_g = -\left.\frac{\partial \angle H_d(\Omega)}{\partial \Omega}\right|_{\Omega=\Omega_0}. \tag{7}$$

Next, our objective is to solve for the coefficients b_n in (4) so that the group delay τ_g is negative. We start from the simplest case, $N = 2$, in which we need two equations to solve for b_1 and b_2. One of the two equations can be directly obtained from (7) by assigning the desired group delay, and the other one can be chosen that the magnitude of the transfer function is normalized to unity, which is

$$|H_d(\Omega = \Omega_0)| = \left|\sum_{n=1}^{2} b_n \cdot e^{-j2n\Omega_0}\right| = 1. \tag{8}$$

Therefore, in this instance, without loss of generality, if we set $\Omega_0 = \pi/2$, $\tau_g = -4$, then by solving (7) and (8) we will have $b_1 = 4$ and $b_2 = 3$. It follows that for an N-stage transversal

TABLE I
COEFFICIENTS FOR MAXIMALLY FLAT NGD RESPONSE

	N=2		N=3			N=4			
τ_{g0}	b_1	b_2	b_1	b_2	b_3	b_1	b_2	b_3	b_4
-1.0	2.5000	1.5000	3.5000	3.5000	1.0000	4.2000	5.4000	2.7000	0.5000
-1.5	2.7500	1.7500	4.0625	4.3750	1.3125	5.0469	7.0656	3.7406	0.7219
-2.0	3.0000	2.0000	4.6667	5.3333	1.6667	6.0000	9.0000	5.0000	1.0000
-3.0	3.5000	2.5000	6.0000	7.5000	2.5000	8.2500	13.7500	8.2500	1.7500
-4.0	4.0000	3.0000	7.5000	10.0000	3.5000	11.0000	19.8000	12.6000	2.8000
-5.0	4.5000	3.5000	9.1667	12.8333	4.6667	14.3000	27.3000	18.2000	4.2000
-6.0	5.0000	4.0000	11.0000	16.0000	6.0000	18.2000	36.4000	25.2000	6.0000
-7.0	5.5000	4.5000	13.0000	19.5000	7.5000	22.7500	47.2500	33.7500	8.2500
-8.0	6.0000	5.0000	15.1667	23.3333	9.1667	28.0000	60.0000	44.0000	11.0000
-9.0	6.5000	5.5000	17.5000	27.5000	11.0000	34.0000	74.8000	56.1000	14.3000
-10.0	7.0000	6.0000	20.0000	32.0000	13.0000	40.8000	91.8000	70.2000	18.2000

	N=5					N=6					
τ_{g0}	b_1	b_2	b_3	b_4	b_5	b_1	b_2	b_3	b_4	b_5	b_6
-1.0	4.7143	7.0714	4.7143	1.5714	0.2143	5.1071	8.5119	6.8095	3.0952	0.7738	0.0476
-1.5	5.8039	9.5594	6.7922	2.3719	0.3352	6.4014	11.7920	10.1074	4.8340	1.2568	0.1396
-2.0	7.0714	12.5714	9.4286	3.4286	0.5000	7.9444	15.8889	14.4444	7.2222	1.9444	0.2222
-3.0	10.2143	20.4286	16.7143	6.5000	1.0000	11.9167	27.0833	27.0833	14.5833	4.1667	0.5000
-4.0	14.3000	31.2000	27.3000	11.2000	1.8000	17.3333	43.3333	46.6667	26.6667	8.0000	1.0000
-5.0	19.5000	45.5000	42.0000	18.0000	3.0000	24.5556	66.1111	75.5556	45.3333	14.1667	1.8333
-6.0	26.0000	64.0000	61.7143	27.4286	4.7143	34.0000	97.1429	116.5714	72.8571	23.5714	3.1429
-7.0	34.0000	87.4286	87.4286	40.0714	7.0714	46.1429	138.4286	173.0357	111.9643	37.3214	5.1071
-8.0	43.7143	116.5714	120.2143	56.5714	10.2143	61.5238	192.2619	248.8095	165.8730	83.1395	7.9444
-9.0	55.3714	152.2714	161.2286	77.6286	14.3000	80.7500	261.2500	348.3333	238.3333	83.4167	11.9167
-10.0	69.2143	195.4286	211.7143	104.0000	19.5000	104.5000	348.3333	476.6667	333.6667	119.1667	17.3333

filter with maximally flat NGD responses, the coefficients b_n can be solved by the following equations with $\Omega_0 = \pi/2$:

$$|H_d(\Omega = \Omega_0)| = \left| \sum_{n=1}^{N} b_n \cdot e^{-j2n\Omega_0} \right| = 1 \tag{9a}$$

$$-\frac{\partial \angle H_d(\Omega)}{\partial \Omega}\bigg|_{\Omega=\Omega_0} = \tau_{g0} \tag{9b}$$

$$-\frac{\partial^{2n-3} \angle H_d(\Omega)}{\partial \Omega^{2n-3}}\bigg|_{\Omega=\Omega_0} = 0, \qquad n = 3, 4 \ldots, (N-1) \tag{9c}$$

Equation (9c) implies that the higher order derivatives of group delay are set to zero in order to obtain a maximally flat response. The results calculated from (9a)–(9c) are listed in Table I, which gives the exact coefficients of maximally flat NGD using transversal-filter topology for $N = 2, 3, 4, 5$, and 6 sections with various amount of NGD (τ_{g0}). It is also noticed that the amount τ_{g0} is in terms of the sampling period T. In this case, the sampling period T is equal to τ_0, and therefore the NGD will become a multiple of τ_0.

Equation (9) has presented a numerical way to solve for the exact coefficients of the problem. In fact, the closed-form solution can be obtained analytically using the same approach for bandpass linear phase filters provided in [17] and [18]. Let $t = \tanh(j\Omega)$, we can then write

$$e^{-j2\Omega} = \frac{1-t}{1+t}. \tag{10}$$

Equation (4) can then be expressed in terms of t as

$$\begin{aligned} H_d &= e^{-j2\Omega} \times \sum_{m=0}^{M=N-1} a_m \cdot e^{-j2m\Omega} \\ &= e^{-j2\Omega} \times \sum_{m=0}^{M=N-1} a_m \cdot \left(\frac{1-t}{1+t}\right)^m \\ &= e^{-j2\Omega} \times \frac{\sum_{m=0}^{M=N-1} a_m (1+t)^{M-m}(1-t)^m}{(1+t)^M} \\ &= e^{-j2\Omega} \times H(t). \end{aligned} \tag{11}$$

It can be proven that the denominator of $H(t)$, i.e.$(1+t)^M$, has a constant delay of M at all frequencies [19]. Furthermore, it has been shown by Rhodes [17] that if the numerator of $H(t)$ has a maximally flat group delay about $t = \infty$, i.e., $\Omega = \pi/2$, it must be of the form of a symmetrical Jacobi polynomial,

$Q_R^{(\alpha)}(t)$, which has a delay of α. The explicit form of $Q_R^{(\alpha)}(t)$ can be expressed as [17]

$$Q_R^{(\alpha)}(t) = \sum_{r=0}^{R} \frac{\binom{R+\alpha}{r}\binom{\alpha-1-r}{R-r}(1+t)^r(1-t)^{R-r}}{2\binom{2R-1}{R}}. \quad (12)$$

Thus, the total delay τ_g of H_d depicted in (11) will be $M - \alpha + 2$ or $N - \alpha + 1$. Furthermore, by comparing (12) and the numerator of $H(t)$ in (11), we can obtain the coefficients

$$a_{N-m-1} = \frac{\binom{N+\alpha-1}{m}\binom{\alpha-1-m}{N-m-1}}{2\binom{2N-3}{N-1}} = b_{N-m} \quad (13)$$

where b_{N-m} refers to the coefficients shown in Fig. 1 and Table I. To give a quantitative example, if we have a transversal filter with $N = 4$ and we let the index $\alpha = 2$, then the total delay will be $4-12+1 = -7$. The coefficients, according to (13), are $(a_0, a_1, a_2, a_3) = (b_1, b_2, b_3, b_4) = (455, 945, 675, 165)/20 = (22.75, 47.25, 33.75, 8.25)$, which results in an identical solution obtained by (9) and listed in Table I for $N = 4$ and $\tau_{g0} = -7$. Therefore, the results of Table I can be double-verified by (13).

IV. Frequency Response

Having derived the coefficients for the maximally flat NGD transversal filters, we would like to examine the frequency responses of the transfer functions using these coefficients.

A. Comparison of Various Sections

As an illustrative example, assuming the sampling period $T = \tau_0 = 0.25$ ns and τ_{g0} is chosen to be -4, we can obtain the corresponding coefficients for different section numbers from Table I.

Fig. 3 plots the frequency responses of the transversal-filter-based NGD circuits with different numbers of section. Since we choose the sampling period to be 0.25 ns, at 1 GHz, the electrical length of each section will become $\pi/2$, which is equal to Ω_0 that we set to solve (9a)–(9c). Therefore, at 1 GHz, the magnitudes of the transfer functions are all unity or 0 dB, as shown in Fig. 3(a). The phases maintain a constant and positive slope around the center frequency of 1 GHz; one can observe that from Fig. 3(b), as the section number increases, the bandwidth of this constant positive slope of phase also increases.

The corresponding group delays for various numbers of sections are plotted in Fig. 4. NGDs with maximally flat responses can be clearly observed from the figure. As a consequence of the phase responses shown in Fig. 3(b), the bandwidth of the flat NGD responses can be augmented when more sections are used in the transversal filter. Moreover, the amount of NGD is 1 ns, which results from the sampling period of 0.25 ns and τ_{g0} of -4 that we choose for this case. It is worth mentioning that the bandwidth of NGD can theoretically be kept increasing by adding more sections to the transversal filter. In addition, it is noted that here we have put effort on making the group delay maximally flat or equivalently generating a linear phase response; on the other hand, however, the amplitude response is uniquely related to the phase response through Hilbert transforms in the case of single input–output path networks, i.e., minimum phase networks [16]. Therefore, in the present case, the amplitude is determined once the condition of maximally flat group delay is imposed. Nevertheless, one can always slightly loosen the maximally flat group-delay condition to adjust the amplitude response so that it can satisfy the desired requirement.

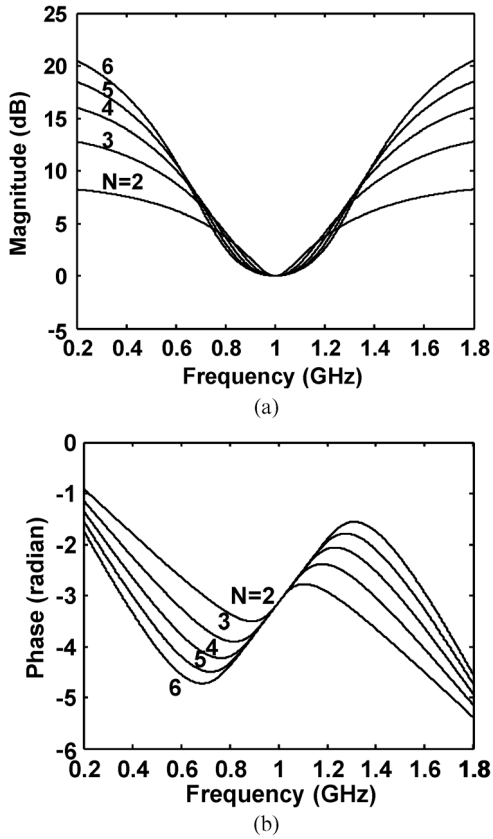

Fig. 3. (a) Amplitude and (b) phase responses of various sections for transversal-filter based NGD circuits.

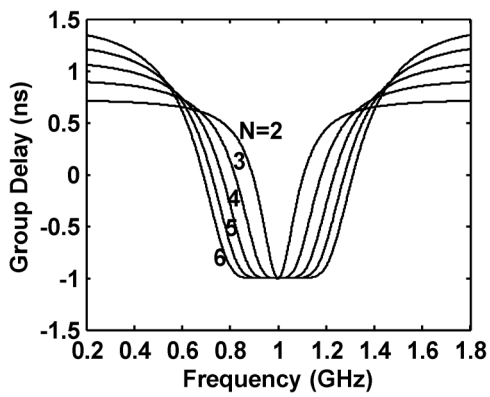

Fig. 4. Group delay of various numbers of sections for transversal filters.

B. z-Domain Analysis

Since the proposed system behaves like a discrete-time system at any instantaneous time frame, we can examine the structure in the z-domain in order to gain qualitative insight

and understanding of it [16]. By letting $e^{j\Omega} = z$, (4) can be expressed as

$$H_d(z) = \sum_{n=1}^{N} b_n \cdot z^{-2n} \tag{14}$$

whose discrete-time domain series can be written as

$$h_d[n] = \sum_{k=1}^{N} b_k \cdot \delta(n-2k). \tag{15}$$

It can then be seen that the system is causal because the impulse response depicted in (15) is zero for $n \leq 0$, which physically means the output of the system solely depends on the past input values. Furthermore, it is apparent that (15) is absolutely summable for finite values of b_k, i.e.,

$$\sum_{n=-\infty}^{\infty} |h_d[n]| < \infty. \tag{16}$$

Therefore, the system is stable as well. In addition, from (14), the region of convergence (ROC) can be defined to include all z, except z is equal to zero.

The characteristics of such type of transversal filter can be further examined by looking at the locations of the zeros of the transfer functions. From (14), the transfer function can be written as

$$H_d(z) = z^{-2N}(b_1 z^{2N-2} + b_2 z^{2N-4} + \cdots + b_N). \tag{17}$$

This implies that the transfer function has $2N-2$ zeros with a $2N$th-order pole located at the origin of the complex z-plane. Furthermore, since the coefficients b_n are real in practice, the zeros must occur in complex conjugate pairs. As a quantitative example, let us consider the case with $N = 2$, then (17) becomes

$$\begin{aligned} H_{d,N=2}(z) &= z^{-4}(b_1 z^2 + b_2) \\ &= z^{-4} b_1 \left(z^2 + \frac{b_2}{b_1} \right) \\ &= \frac{(z-z_1)(z-z_2)}{(z-p_1)(z-p_2)(z-p_3)(z-p_4)}. \end{aligned} \tag{18}$$

It can be found that this second-order system will have four poles (p_1, p_2, p_3, p_4) at the origin and two zeros, $z_{1,2} = \pm j\sqrt{b_2/b_1}$, at the imaginary axis, as shown in Fig. 5. The frequency response can be obtained by evaluating the transfer function on the unit circle of z-plane, which is equivalently obtained by substituting z with $e^{j\Omega}$into (18). As also depicted in Fig. 5, the magnitude and phase response can be defined as

$$|H_{d,N=2}(\Omega)| = \frac{M_1 M_2}{m_1^4} = M_1 M_2 \tag{19a}$$

$$\angle H_{d,N=2}(\Omega) = \theta_1 + \theta_2 - 4\,\Omega \tag{19b}$$

where (M_i, θ_i) and (m_i, Ω) are the magnitude and phase of zero and pole vectors, respectively. Since all the poles are at the origin, the magnitudes of pole vectors are all unity and the phases are equal to Ω. The group delay can be obtained by taking derivative of (19b), which then becomes

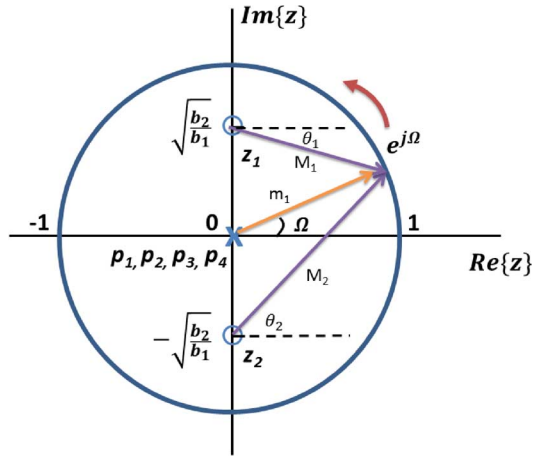

Fig. 5. Pole-zero plot for a second-order system $(N = 2)$ described in (18).

$$\tau_{g,N=2} = -\frac{\partial \angle H_{d,N=2}(\Omega)}{\partial \Omega} = -\frac{\partial \theta_1}{\partial \Omega} - \frac{\partial \theta_2}{\partial \Omega} + 4. \tag{20}$$

In order to obtain NGD, it follows that (20) needs to be negative. From direct inspection, the rate of phase change $(\partial\theta_1/\partial\Omega)$ becomes maximum when $\Omega = \pi/2$ since M_1 is minimum at this frequency. Hence, if $\partial\theta_1/\partial\Omega$ is big enough, then it is possible for (20) to become negative. Furthermore, at $\Omega = \pi/2$, the relation between infinitesimal frequency $(\Delta\Omega)$ and phase $(\Delta\theta)$ can be expressed as

$$\Delta\Omega = \Delta\theta_1 \cdot M_1 = \Delta\theta_2 \cdot M_2. \tag{21}$$

Therefore, we can rewrite (20) for NGD,

$$\tau_{g,N=2} = -\frac{\partial \theta_1}{\partial \Omega} - \frac{\partial \theta_2}{\partial \Omega} + 4 = -\frac{1}{M_1} - \frac{1}{M_2} + 4 < 0. \tag{22}$$

Using the fact that $M_1 = 1 - \sqrt{b_2/b_1}$ and $M_2 = 1 + \sqrt{b_2/b_1}$, from (22) we will have

$$\sqrt{\frac{b_2}{b_1}} > 0.707 \text{ or } \frac{b_2}{b_1} > 0.5. \tag{23}$$

Equation (23) states that the zeros need to be close enough to the unit circle at least for a certain distance. It can also be seen that the coefficients for $N = 2$ provided in Table I all satisfy this criteria. Moreover, from Fig. 5 and (19a), we can find that the amplitude of the transfer function is decreasing as it approaches the zero with respect to the frequency and it reaches the minimum at $\Omega = \pi/2$ when NGD occurs, which agrees with the previous findings that NGD will happen at the range of frequencies where the absorption or the attenuation is maximum [2]. From another point of view, this is because zeros inside the unit circle can essentially give us an increasing phase as the frequency increases, which is necessary in order to produce NGD.

Fig. 6 plots the poles and zeros of the transfer functions for various sections (N) with maximally flat NGD characteristics,

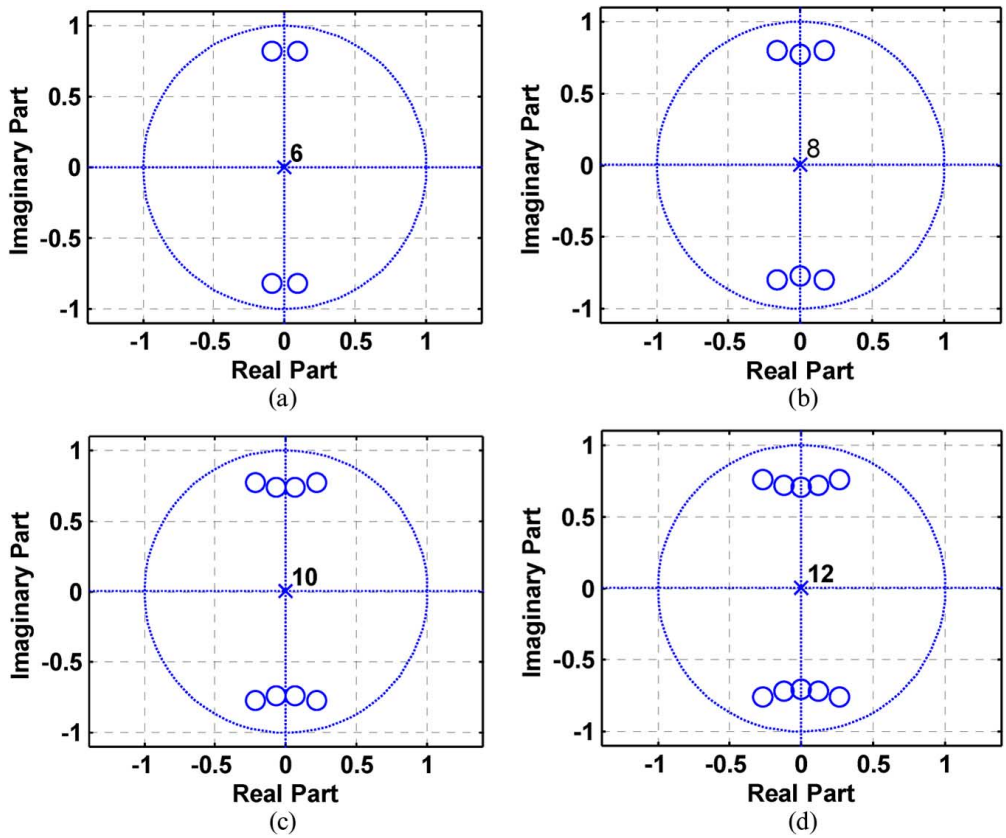

Fig. 6. Pole-zero plots in z-plane for $\tau_{g0} = -4$ of: (a) $N = 3$, (b) $N = 4$, (c) $N = 5$, and (d) $N = 6$.

which use the coefficients listed in Table I with a NGD of -4. It is interesting that from Fig. 6 we can see when N increases, the number of zeros also increases along the unit circle near $\Omega = \pi/2$, which results in a broader bandwidth of a flat NGD. From Figs. 4 and 6, it can be inferred that the bandwidth of NGD can be theoretically increased as we have a greater number of sections in the transversal filter. The price that we pay here for broadband NGD is that the difference of magnitude between in-band and out-of-band will become huge when more sections are used, as can also be found in Fig. 3(a), which also corresponds to the results reported in [20].

From the above discussion, we could conclude the following facts.

1) The zeros must be inside the unit circle of the z-plane and close enough to the periphery in order to generate NGD.
2) The magnitude of the transfer function becomes minimum during NGD.
3) More zeros are needed in the case of larger N with broader bandwidth of NGD.

V. Implementation I: Passive Approach

A. Multi-Section Directional Coupler

A simple realization of a passive transversal filter in microwave regimes is to use a multi-section directional coupler, as shown in Fig. 7. Assuming that the coupling is weak ($C_n \leq -10$ dB) and each section is a quarter-wavelength long ($\theta = \pi/2$) at the center frequency, the total voltage transfer

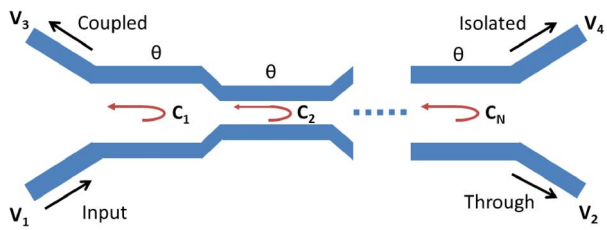

Fig. 7. N-section directional coupler.

function of the coupled port of an N-section multisection directional coupler can be expressed as [21]

$$\frac{V_3}{V_1} = \sum_{n=1}^{N} (jC_n \sin\theta) e^{-j(2n-1)\theta} \tag{24}$$

where C_n is the coupling factor for the nth section of the directional coupler, and θ is the electrical length of coupled lines. It is noted that (24) has a similar mathematical form as (4) if we map θ to Ω. Although the coefficients of (24) have a $j\sin\theta$ dependency, it will not affect the mutual ratios among each coefficients since the $j\sin\theta$ dependency will be cancelled out. The main difference between (24) and (4) is that since (24) starts from $e^{-j\theta}$ instead of $e^{-j2\theta}$, it will have one less pole compared to (4), which will result in an NGD increased by one sampling period. Using (24), Fig. 8 plots the group delays in terms of the sampling periods versus the electrical length θ for various sections of directional couplers in which the coupling factors are the same as the coefficients used in Section IV, i.e., those for

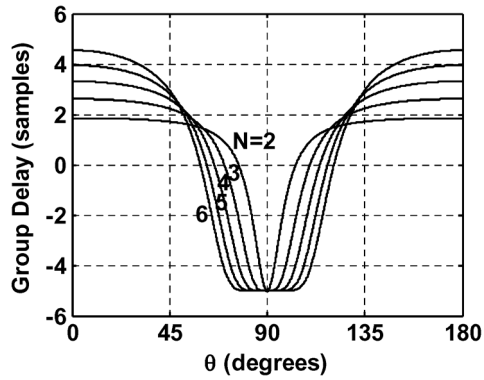

Fig. 8. Group delays of various sections of direction coupler calculated from (24).

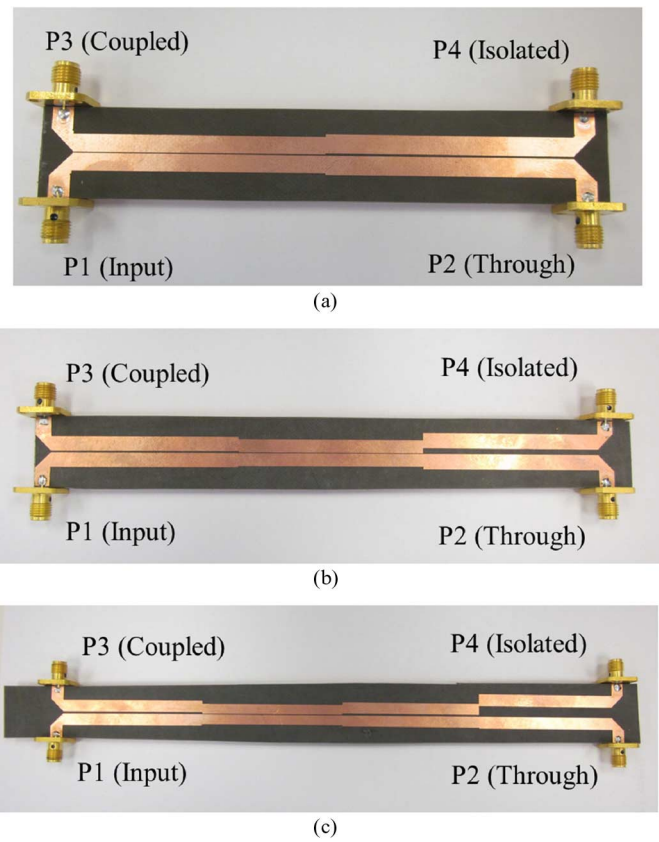

Fig. 9. Prototypes of NGD circuits based on multi-section directional couplers for: (a) $N = 2$, (b) $N = 3$, and (c) $N = 4$.

$\tau_{g0} = -4$. From Fig. 8, we can find that the NGD increases by one sampling period to -5 as mentioned above, and we also observe that as more sections of directional coupler are used, the bandwidth of NGD will increase accordingly.

B. Prototypes and Results

To verify the NGD circuits based on transversal-filter concepts, we fabricated three different microstrip line-based multi-section directional couplers for $N = 2, 3$, and 4, respectively, as shown in Fig. 9. The prototypes are fabricated using RT/Duroid 5880 substrates with a dielectric constant of 2.2 and thickness

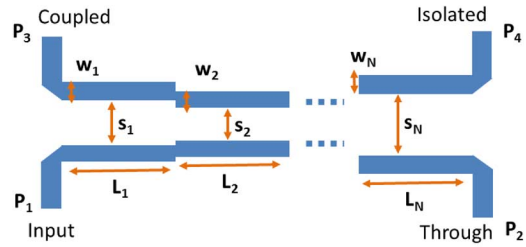

	L_1	W_1	s_1	L_2	W_2	s_2
N=2	55.71	3.99	0.18	55.42	4.36	0.43
N=3	55.42	4.35	0.47	55.71	3.99	0.14
N=4	55.16	4.59	0.85	55.71	3.99	0.24

	L_3	W_3	s_3	L_4	W_4	s_4
N=3	54.93	4.74	1.66			
N=4	55.27	4.49	0.69	54.69	4.84	4.27

Fig. 10. Dimensions of an N-section directional coupler (unit: millimeters).

of 62 mils. The dimensions of the various directional couplers are summarized in Fig. 10.

The coupling factors for different sections of directional couplers ($z = 2, 3, 4$) are based on the coefficients listed in Table I for $\tau_{g0} = -4$, as shown in (25), in which the maximum coefficients are normalized to -10 dB, which is 0.3162 in linear scale,

$$\mathbb{C}_{N=2} = [0.3162, 0.2372] \tag{25a}$$
$$\mathbb{C}_{N=3} = [0.2372, 0.3162, 0.1107] \tag{25b}$$
$$\mathbb{C}_{N=4} = [0.1757, 0.3162.0.2012, 0.0447]. \tag{25c}$$

It is noted that the coefficients in (25) are calculated from the ideal transversal filters and should be used as a starting point to find out the actual dimensions of the directional couplers shown in Fig. 10. To elaborate further, although (24) is a good approximation for a multi-section directional coupler with a low coupling ratio, it might not accurately reflect the phase response due to the tiny secondary coupling from the output line to input line; this can be an issue especially when the coupling is strong since the phase response is more sensitive than the amplitude response. Therefore, in practice, it is necessary to do a post-layout optimization of the structure with a full-wave simulation using the ideal coefficients given in Table I as starting numbers. On the other hand, in order to obtain the exact solution, one can use the well-known four-port coupler to two-port stepped impedance transformation to analyze the problem for higher coupling ratio and to take into account the secondary coupling issue [22]. The detailed procedure is shown in the Appendix.

The center frequency of the directional couplers is designed to be 1 GHz, which means the electrical length θ is $\pi/2$ at 1 GHz. Fig. 11 shows the simulated results using the 3-D planar electromagnetic simulator Momentum provided in the Advanced Design System (ADS) for the NGD circuits based on multi-section directional couplers. We can see from Fig. 11(a) that the magnitudes of S_{31} decreases to the minimum at around 1 GHz, which corresponds to the previous discussion in Section IV. The phases of S_{31}, as shown in Fig. 11(b), change the sign of slope near the center frequency, indicating the NGDs occurs in the region. One can also find out that as more sections are used, the frequency band in which the

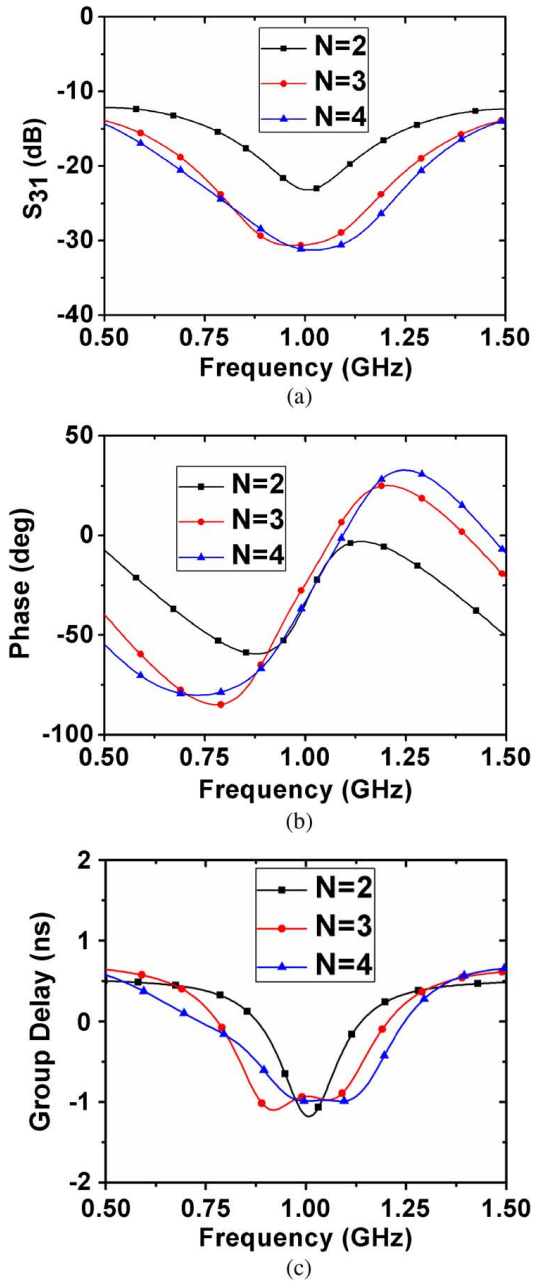

Fig. 11. Simulated response of: (a) amplitude, (b) phase, and (c) group delay for NGD circuits based on multi-section directional couplers.

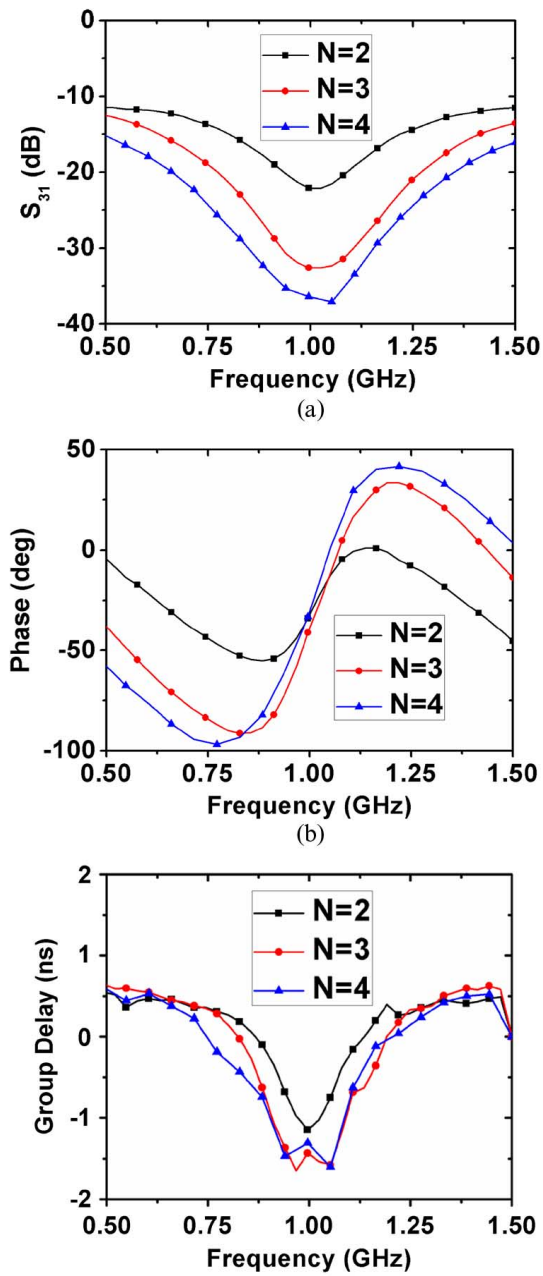

Fig. 12. Measured response of: (a) amplitude, (b) phase, and (c) group delay for NGD circuits based on multi-section directional couplers.

phase reverses its sign also becomes broader, implying a wider bandwidth of NGD. The simulated group delays from port 1 to port 3 for different sections of directional coupler can be seen in Fig. 11(c). It shows that the NGD is around -1 ns at the center frequency of 1 GHz. In addition, when the number of sections N increases, a larger bandwidth of NGD can be observed. Furthermore, by using the proper coupling coefficients derived above, a flat response of NGD can be realized.

The measured results are plotted in Fig. 12. Compared to the simulated results shown in Fig. 11, they agree reasonably well. The magnitude of S_{31} decreases more in the measured results, especially when more sections are used, as can be seen in Fig. 12(a). This may be due to more loss introduced in the actual fabricated prototypes. The reversed sign of slope for the phase of S_{31} can also be observed in Fig. 12(b), in which the slopes for $N = 3$ and $N = 4$ become steeper compared to the simulation. As a result, the measured group delays for $N = 3$ and $N = 4$ cases become around -1.5 ns at the center frequency of 1 GHz. This might be due to the handmade fabrication errors. Overall, with more sections used in directional couplers, the bandwidth of NGD increases. Moreover, as mentioned above, a flat response of NGD can be achieved by using the proper coupling coefficients for each section of the directional coupler.

The other S-parameters, such as return loss (S_{11}), through port insertion loss (S_{21}) and isolation (S_{41}) are also plotted in Fig. 13. The simulation and measurement show a good agreement, which indicates that the proposed multi-section directional couplers have good return loss (>20 dB) and good isolation (>15 dB) and small insertion loss at the NGD region.

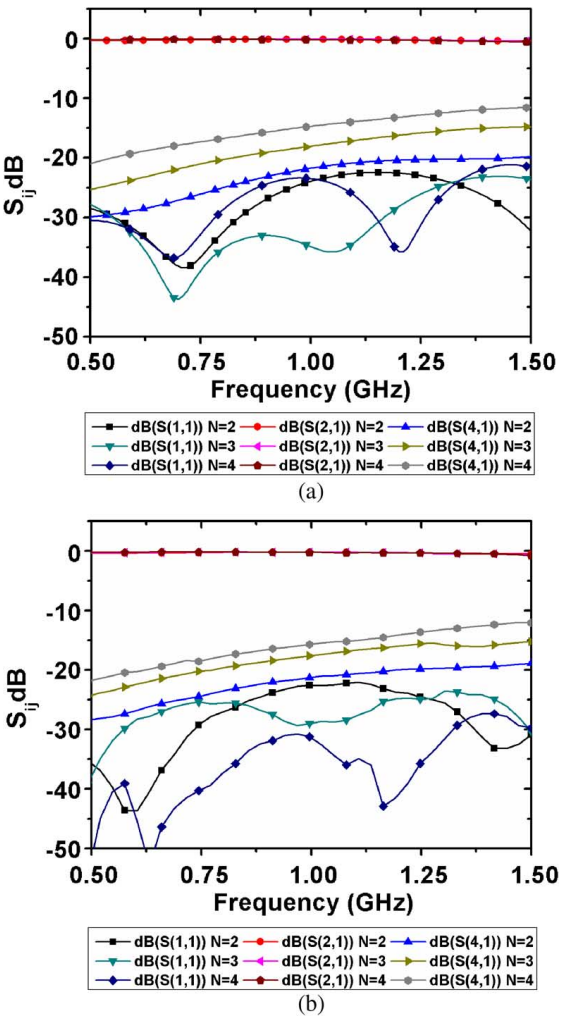

Fig. 13. (a) Simulated and (b) measured S-parameters for various sections of directional couplers.

These properties can make the devices useful when installed prior to the input of the circuitries because it can reduce the excessive group delay due to the compensation of NGD. For instance, the proposed NGD devices can be potentially used in dynamic power supply or envelope tracking of power amplifiers (PAs) [23], [24]. In a supply modulated PA, it is important that the dynamic power supply can accurately track the signal envelope to maximize the overall efficiency. The coupled port of the proposed directional coupler-based NGD circuit can be connected to the detector path in order to compensate the time mismatch between the dynamic power supply and the signal envelope, whereas the through port can be directly linked to the RF signal path. As a result, the PA efficiency can be further enhanced [25].

VI. Implementation II: Active Approach

A. DAs With NGD

Although a multi-section directional coupler can provide a very simple way to realize the form of a transversal filter, it suffers from tremendous loss in the NGD region, especially when an NGD-bandwidth product is large since the out-of-band gain needs to be large as well [20]. DAs stand out as an excellent

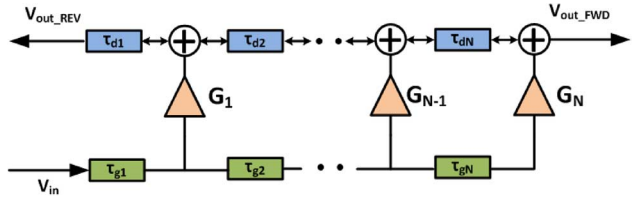

Fig. 14. N-stage DA.

choice to provide amplification for the NGD circuits, being essentially one type of transversal-filer in active fashion. Fig. 14 illustrates the diagram of an N-stage DA in which G_k is the gain coefficient of the kth tap amplifier, τ_{gk} and τ_{dk} indicate the time delay of the kth section of the gate line and drain line, respectively. Furthermore, if we choose that $\tau_{gi} = \tau_{di} = \tau_0$, then the transfer functions of the forward and reverse port with respect to the input can be expressed as [12]

$$H_{\rm FWD}(\omega) = \frac{V_{\rm out\_FWD}}{V_{\rm in}} = \sum_{k=1}^{N} G_k e^{-j\omega(N\tau_0)} \tag{26a}$$

$$H_{\rm REV}(\omega) = \frac{V_{\rm out\_REV}}{V_{\rm in}} = \sum_{k=1}^{N} G_k e^{-j\omega(2k\tau_0)}. \tag{26b}$$

One can immediately identify that (26b) has the same mathematical form as (4) and can further observe that if we use the coefficients that we have derived in Table I for the gain coefficients G_k in (26), we will have a NGD response at the DA's reverse port, while maintaining a flat gain at its forward port as G_k's merely sum up constructively, as indicated in (26a).

It is noted that the coefficients G_k are in fact related and proportional to the transconductance (g_m) of an active device. Therefore, the idea can be quickly examined using the circuit simulator in ADS for the ideal situation. Fig. 15 shows the schematics in ADS for a two-stage DA in which the unit-cell contains ideal transmission lines with the characteristic impedance of 50 Ω and phase of 90°, as well as an ideal voltage-control-current-source (VCCS) with a transconductance of g_m (S). Furthermore, if we choose the amounts of g_m for the two-stage to be large enough as (0.4 S, 0.3 S), obtained from Table I ($N = 2$, $\tau_{g0} = -4$) with a factor of one-tenth, then we will obtain the responses shown in Fig. 16. Fig. 16(a) plots the forward (S_{41}) and reverse gain (S_{31}) of the DA; as expected, the reverse gain reaches minimum at the center frequency of 1 GHz during the NGD region, as seen in Fig. 16(b), whereas the forward gain maintains a flat response. It can be seen that if the trans-conductance of active devices are large enough, even though the reverse gain reaches the minimum, it will still have gain. In fact, the NGD-bandwidth product is proportional to the maximum of the out-of-band gain [20]; it follows that if the NGD-bandwidth product is small, then it does not require so much gain from the amplifiers.

B. Prototypes and Results

As a proof-of-concept, we fabricated a DA using commercial off-the-shelf discrete transistors NEC NE3210S01. As shown in Fig. 17, the DA contains two transistors with individual gate biases to form a two-stage NGD circuit. The electrical length

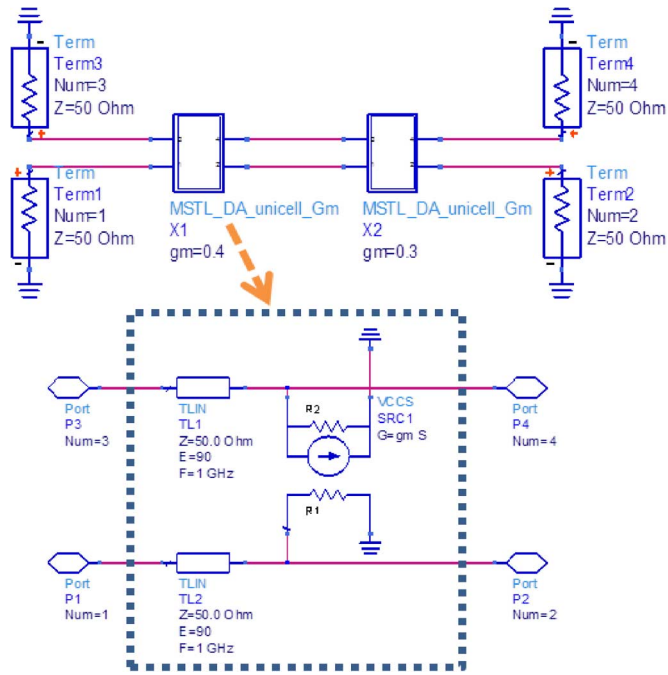

Fig. 15. Schematics of an ideal two-stage DA.

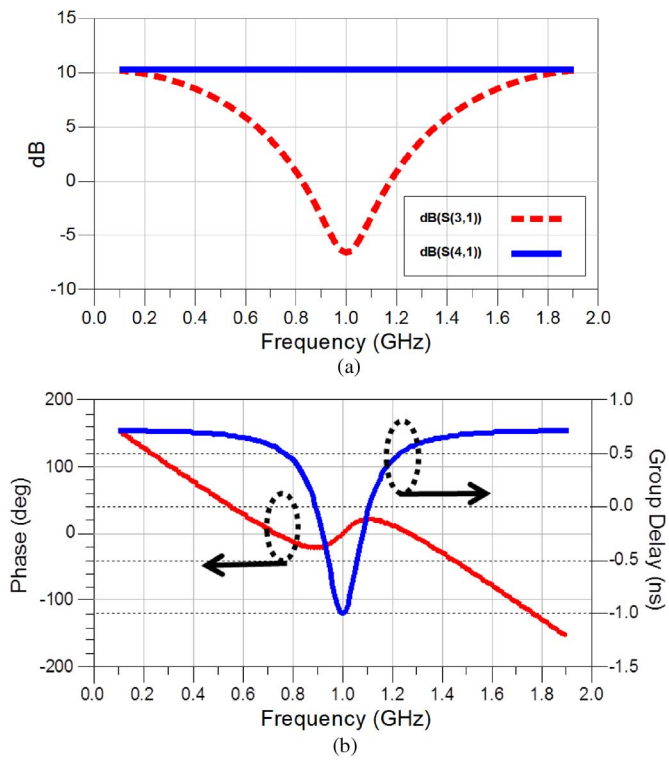

Fig. 16. Simulated: (a) forward and reverse gain and (b) phase response and group delay at the reverse port of an ideal DA.

between each stage is designed to be a quarter-wavelength at the center frequency of 1 GHz. The biasing circuitry of the unit-cell is based on lumped components in order to miniaturize the circuit size, as shown in Fig. 18; DC decoupling capacitors are

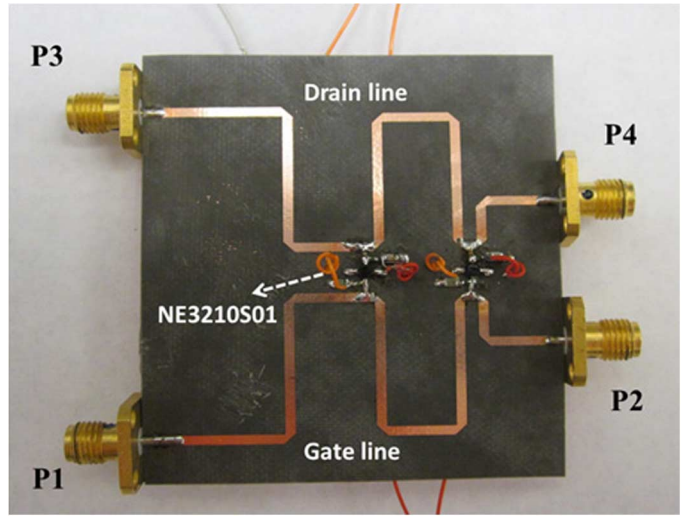

Fig. 17. Prototype of a two-stage NGD circuits based on DAs.

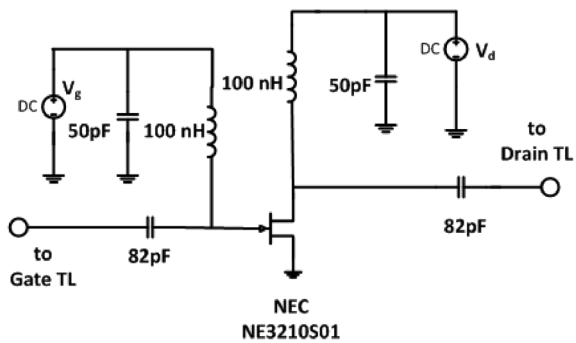

Fig. 18. Biasing circuitry of a gain unit-cell.

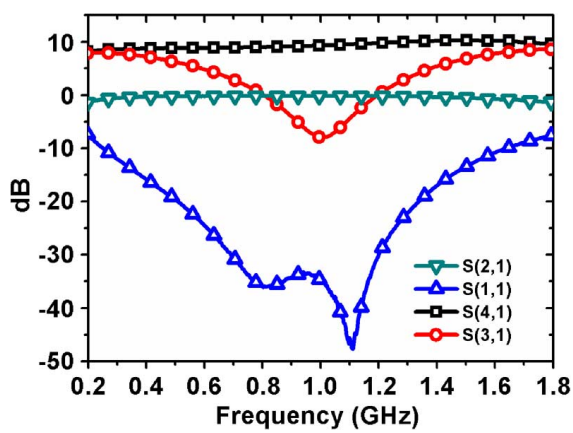

Fig. 19. Measured S-parameters of the fabricated two-stage NGDDA.

used to connect the gate and drain of the transistor, whereas inductors are used to carry out dc bias and RF block.

The maximum transconductance of NE3210S01, according to the data sheet, can be found to be around 0.075 S in which the bias condition is $V_g = -0.3$ V and $V_d = 2$ V; therefore, we use this number as the maximum in our gain coefficients calculation. Fig. 19 shows the measured S-parameters of the fabricated two-stage DA. As expected, the forward gain shows a flat

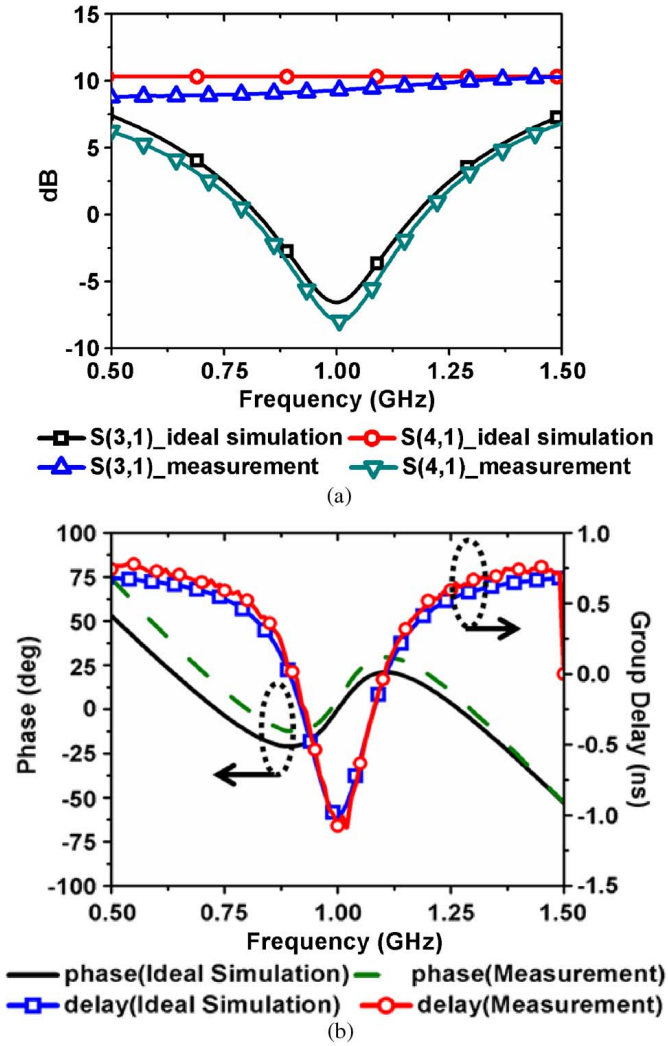

Fig. 20. Comparison between the ideal circuit simulation and measured results of the two-stage NGDDA.

response of around 10-dB gain, whereas the reverse gain has a minimum of -7.8 dB at the center frequency 1 GHz where NGD occurs. In addition, the return loss is greater than 30 dB and the insertion loss is around 0.2 dB in the frequency of interest. We then compared the ideal circuit simulation using the topology in Fig. 15 with the measured results; since the maximum transconductance of the transistors we use is 0.075 S, the amounts of g_m in the circuit simulation are (0.075 S, 0.05625 S). The comparison is plotted in Fig. 20 in which the bias condition in the measurement is $V_{g1} = 0.3$ V, $V_{g2} = -0.39$ V, and $V_d = 2$ V. Fig. 20(a) shows the forward and reverse gain of the DA; the measured results agree very well with the ideal circuit simulation. The phase and group delay of the DA are plotted in Fig. 20(b), indicating a great agreement between the ideal circuit simulation and measurement. The maximum group delay of the two-stage DA is -1 ns at 1 GHz and the NGD region of which is 0.9–1.1 GHz.

VII. Conclusion

In this paper, we proposed a comprehensive method to synthesize NGD circuits in microwave regimes based on transversal-filter principles. We analytically derive the coefficients that are desired to form maximally flat responses of NGD. We have demonstrated both passive and active realization of the proposed NGD circuits. By choosing the appropriate coupling coefficients, we are able to realize the NGD at the coupled port of a multi-section directional coupler as well as the reverse port of a DA. The proposed method provides a simple way to create a broadband NGD with a flat response. Moreover, one of the advantages for the proposed passive NGD circuits is that they do not need any lumped components and therefore are very suitable to be used in high-frequency integrated circuits in which lumped components are not obtainable. The proposed NGD methodology is expected to be applied in microwave systems such as in dynamic power supply or envelope-tracking schemes of PAs in order to eliminate excessive group delay of the envelope path. In addition, it is worth mentioning that the coefficients derived in this work can directly be applied to digital finite impulse response (FIR) filters to provide corresponding NGD responses.

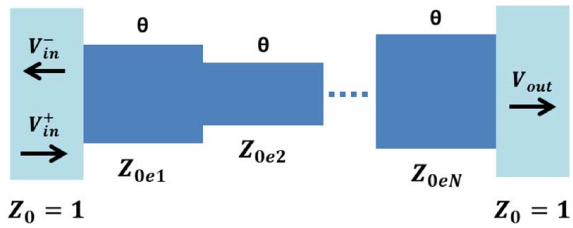

Fig. 21. N-stage quarter-wavelength stepped-impedance transformer.

Appendix

The problem illustrated in Fig. 7 can be transformed to an N-stage quarter-wavelength stepped-impedance transformer, as shown in Fig. 21, in which the transmission matrix can be defined in terms of the characteristic impedances [22], given the reference impedance Z_0 is normalized to unity,

$$\prod_{k=1}^{N}\begin{bmatrix}\cos\theta & jZ_{0ek}\sin\theta\\ \left(\frac{j}{Z_{0ek}}\right)\sin\theta & \cos\theta\end{bmatrix}=\begin{bmatrix}A_n & jB_n\\ jC_n & D_n\end{bmatrix}. \quad (27)$$

Furthermore, by mapping V_1 to V_{in}^+ and V_3 to V_{in}^-, the transfer function describe in (24) will now be transformed to the reflection coefficient, and according to (27), it can be expressed as

$$\Gamma=\frac{V_{\text{in}}^-}{V_{\text{in}}^+}=\frac{(A_n-D_n)+j(B_n-C_n)}{(A_n+D_n)+j(B_n+D_n)}. \quad (28)$$

It follows that the phase term of (28) can be obtained as

$$\angle\Gamma=\tan^{-1}\frac{B_n-C_n}{A_n-D_n}-\tan^{-1}\frac{B_n+C_n}{A_n+D_n}. \quad (29)$$

The procedure to obtain maximally flat NGD is then similar to (9), namely, to solve for the following equations in order to find the desired impedances (Z_{0ek}) for each stage:

$$\left|\Gamma\left(\theta=\frac{\pi}{2}\right)\right|=\Gamma_0 \quad (30a)$$

$$-\left.\frac{\partial \angle\Gamma(\theta)}{\partial\theta}\right|_{\theta=\frac{\pi}{2}} = \tau_{g0} \tag{30b}$$

$$-\left.\frac{\partial^{2n-3}\angle\Gamma(\theta)}{\partial\theta}\right|_{\theta=\frac{\pi}{2}} = 0, \qquad n = 3, 4\ldots, (N-1). \tag{30c}$$

To give a quantitative example, assuming the impedance transformer has three stages ($N = 3$), and also we let $\Gamma_0 = 0.04$ and $\tau_{g0} = -4$, then by solving (30), we can obtain

$$[Z_{0e1}, Z_{0e2}, Z_{0e3}] = [1.27094, 1.34942, 1.1051]. \tag{31}$$

Using the relation between the coupling coefficient and the even-mode characteristic impedance [21], we have

$$C_k = \frac{Z_{0ek}^2 - 1}{Z_{0ek}^2 + 1}. \tag{32}$$

Thus, from (31) and (32), the coupling coefficients are calculated to be $C = [0.2352, 0.2910, 0.0996]$. Compared to $\mathbb{C}_{N=3} = [0.2372, 03162, 0.1107]$ shown in (25b), we can find out these two sets of coefficients are very close, indicating (24) can serve as a good approximation to the exact solution obtained here when the coupling is small enough. It is noted that if the coupling ratios are large (typically larger than -10 dB), then (24) is no longer accurate since the secondary coupling is strong and needs to be taken into account. From another perspective, with weak coupling ratios, a passive multi-section directional coupler can be approximated as a transversal filter or a FIR filter; in the case of strong coupling ratios, the multi-section directional coupler should be treated as a recursive filter or an infinite impulse response (IIR) filter, and therefore should be solved by using the method provided here. On the other hand, for an active NGD circuit using DAs, because active devices are unilateral, there is no secondary coupling, and therefore it should always behave as a transversal filter or FIR filter.

ACKNOWLEDGMENT

The authors thank C.-Y. Lou, Wireless Integrated Systems Research Group, University of California at Los Angeles (UCLA), Los Angeles, CA, USA, for the advice on discrete-time signal processing. The authors would also like to thank Dr. T.-Y. Chen, Dr. S. Gharavi, and Prof. B. Daneshrad, all with UCLA, for their kind help and suggestions.

REFERENCES

[1] L. Brillouin, *Wave Propagation and Group Velocity*. New York, NY, USA: Academic, 1960.
[2] E. L. Bolda and R. Y. Chiao, "Two theorems for the group velocity in dispersive media," *Phys. Rev. A, Gen. Phys.*, vol. 48, no. 5, pp. 3890–3894, Nov. 1993.
[3] M. W. Mitchell and R. Y. Chiao, "Negative group delay and 'fronts' in a causal system: An experiment with very low frequency bandpass amplifiers," *Phys. Lett. A*, vol. 230, pp. 133–138, Jun. 1997.
[4] M. W. Mitchell and R. Y. Chiao, "Causality and negative group delays in a simple bandpass amplifier," *Amer. J. Phys.*, vol. 66, pp. 14–19, Jan. 1998.
[5] M. Kitano, T. Nakanishi, and K. Sugiyama, "Negative group delay and superluminal propagation: An electronic circuit approach," *IEEE J. Sel. Topics Quantum Electron.*, vol. 9, no. 1, pp. 43–51, Jan. 2003.
[6] B. Ravelo, A. Perennec, and M. Le Roy, "Synthesis of broadband negative group delay active circuits," in *IEEE MTT-S Int. Microw. Symp. Dig.*, Jun. 2007, pp. 2177–2180.
[7] H. Noto, K. Yamauchi, M. Nakayama, and Y. Isota, "Negative group delay circuit for feed-forward amplifier," in *IEEE MTT-S Int. Microw. Symp. Dig.*, Jun. 2007, pp. 1103–1106.
[8] H. Choi, Y. Jeong, J. Lim, S. Y. Eom, and Y. B. Jung, "A novel design for a dual-band negative group delay circuit," *IEEE Microw. Wireless Compon. Lett.*, vol. 21, no. 1, pp. 19–21, Jan. 2011.
[9] S. Lucyszyn. I. D. Robertson and A. H. Aghvami, "Negative group delay synthesiser," *Electron. Lett.*, vol. 29, no. 9, pp. 798–800, Apr. 1993.
[10] M. Kandic and G. E. Bridges, "Asymptotic limits of negative group delay in active resonator-based distributed circuits," *IEEE Trans. Circuits Syst. I, Reg. Papers*, vol. 58, no. 8, pp. 1727–1735, Aug. 2011.
[11] O. Siddiqui, M. Mojahedi, and G. Eleftheriades, "Periodically loaded transmission line with effective negative refractive index and negative group velocity," *IEEE Trans. Microw. Theory Techn.*, vol. 52, no. 5, pp. 1449–1454, May 2004.
[12] C.-T. M. Wu, S. Gharavi, B. Daneshrad, and T. Itoh, "A dual-purpose reconfigurable negative group delay circuit based on distributed amplifiers," *IEEE Microw. Wireless Compon. Lett.*, vol. 23, no. 11, pp. 593–595, Nov. 2013.
[13] A. Borjak, P. P. Monteiro, J. J. O'Reilly, and I. Darwazeh, "High speed generalized distributed-amplifier-based transversal-filter topology for optical communication systems," *IEEE Trans. Microw. Theory Techn.*, vol. 45, no. 8, pp. 1453–1457, Aug. 1997.
[14] C. Rauscher, "Microwave active filter based on transversal and recursive principles," *IEEE Trans. Microw. Theory Techn.*, vol. MTT-33, no. 12, pp. 1350–1360, Dec. 1985.
[15] C.-T. M. Wu, S. Gharavi, and T. Itoh, "Negative group delay circuit based on a multisection asymmetrical directional coupler," in *Asia–Pacific Microw. Conf.*, Seoul, Korea, Nov. 2013, pp. 333–335.
[16] A. V. Oppenheim, R. W. Schafer, and J. R. Buck, *Discrete-Time Signal Processing*, 2nd ed. Upper Saddle River, NJ, USA: Prentice-Hall, 1999.
[17] J. D. Rhodes, "The design and synthesis of a class of bandpass linear phase filters," *IEEE Trans. Microw. Theory Techn.*, vol. MTT-17, no. 4, pp. 189–204, Apr. 1969.
[18] T. A. Abele, "Transmission line filters approximating a constrained delay in a maximally flat sense," *IEEE Trans. Circuit Theory*, vol. CT-14, no. 3, pp. 298–306, Sep. 1967.
[19] S. O. Scanlan and J. D. Rhodes, "Microwave networks with constant delay," *IEEE Trans. Circuit Theory*, vol. CT-14, no. 3, pp. 290–297, Sep. 1967.
[20] M. Kandic and G. E. Bridges, "Limits of negative group delay phenomenon in linear causal media," *Progr. Electromagn. Res.*, vol. 134, pp. 227–246, 2013.
[21] D. M. Pozar, *Microwave Engineering*, 3rd ed. Toronto, ON, Canada: Wiley, 2005.
[22] R. Levy, "General synthesis of asymmetric multi-element coupled-transmission-line directional couplers," *IEEE Trans. Microw. Theory Techn.*, vol. MTT-11, no. 4, pp. 226–237, Jul. 1963.
[23] B. Kim, J. Moon, and I. Kim, "Efficiently amplified," *IEEE Microw. Mag.*, vol. 11, no. 5, pp. 87–100, Aug. 2010.
[24] E. McCune, "Envelope tracking or polar-which is it?," *IEEE Microw. Mag.*, vol. 13, no. 4, pp. 34–56, Jun. 2012.
[25] F. Wang, A. Yang, D. Kimball, L. Larson, and P. Asbeck, "Design of wide bandwidth envelope tracking power amplifiers for OFDM applications," *IEEE Trans. Microw. Theory Techn.*, vol. 53, no. 4, pp. 1244–1255, Apr. 2005.

Chung-Tse Michael Wu (S'10) received the B.S. degree in electrical engineering from National Taiwan University (NTU), Taipei, Taiwan, in 2006, the M.S. degree in electrical engineering from the University of California at Los Angeles (UCLA), Los Angeles, CA, USA, in 2009, and is currently working toward the Ph.D. degree in electrical engineering at UCLA.

Since September 2008, he has been a Graduate Student Researcher with the Microwave Electronics Laboratory, UCLA. In 2009, he was a Summer Intern with Bell Labs, Alcatel-Lucent, Murray Hills, NJ, USA. In 2012, he was a Special-Joint Researcher with the Japan Aerospace

Exploration Agency (JAXA), Kanagawa, Japan. He is a reviewer for several microwave journals including *IET* and *PIER*. His research interests include applied electromagnetics, antennas, passive/active components, microwave systems, and metamaterials.

Mr. Wu is a Student Member of the IEEE Microwave Theory and Techniques Society (IEEE MTT-S) and the IEEE Communications Society (ComSoc). He is a reviewer for the IEEE TRANSACTIONS ON MICROWAVE THEORY AND TECHNIQUES. He was the recipient of the 2011 Asia–Pacific Microwave Conference (APMC) Student Prize and 2013 APMC Best Student Paper Award.

Tatsuo Itoh (S'69–M'69–SM–74-F'82–LF'06) received the Ph.D. degree in electrical engineering from the University of Illinois at Urbana-Champaign, Urbana, IL, USA, in 1969.

From September 1966 to April 1976, he was with the Electrical Engineering Department, University of Illinois at Urbana-Champaign. From April 1976 to August 1977, he was a Senior Research Engineer with the Radio Physics Laboratory, SRI International, Menlo Park, CA, USA. From August 1977 to June 1978, he was an Associate Professor with the University of Kentucky, Lexington, KY, USA. In July 1978, he joined the faculty of The University of Texas at Austin, Austin, TX, USA, where he became a Professor of electrical engineering in 1981 and Director of the Electrical Engineering Research Laboratory in 1984. During the summer of 1979, he was a Guest Researcher with AEG-Telefunken, Ulm, Germany. In September 1983, he was selected to hold the Hayden Head Centennial Professorship of Engineering at The University of Texas at Austin. In September 1984, he became the Associate Chairman for Research and Planning, Electrical and Computer Engineering Department, The University of Texas at Austin. In January 1991, he joined the University of California at Los Angeles (UCLA), Los Angeles, CA, USA, as Professor of electrical engineering and Holder of the TRW Endowed Chair in Microwave and Millimeter Wave Electronics (currently the Northrop Grumman Endowed Chair). He was an Honorary Visiting Professor with the Nanjing Institute of Technology, Nanjing, China, and with the Japan Defense Academy. From 1994 to 1996, he was the Adjunct Research Officer with the Communications Research Laboratory, Ministry of Post and Telecommunication, Japan. He was a Visiting Professor with The University of Leeds, Leeds, U.K. From 2010 to 2012, he was the Research Chair with National Taiwan University. He has authored or couathored 428 journal publications and 864 refereed conference presentations. He has authored 48 books/book chapters in the area of microwaves, millimeter waves, antennas, and numerical electromagnetics. He has generated 78 Ph.D. students.

Dr. Itoh is a member of the Institute of Electronics and Communication Engineers of Japan and Commissions B and D, USNC/URSI. He was the editor-in-chief of the IEEE TRANSACTIONS ON MICROWAVE THEORY AND TECHNIQUES (1983–1985). He serves on the Administrative Committee of the IEEE Microwave Theory and Techniques Society (IEEE MTT-S). He was president of the IEEE MTT-S (1990). He was the editor-in-chief of IEEE MICROWAVE AND GUIDED WAVE LETTERS (1991–1994). He was elected an Honorary Life Member of the IEEE MTT-S (1994). He was inducted to National Academy of Inventors as a Fellow (2014). He was the chairman of USNC/URSI Commission D (1988–1990) and of Commission D, International URSI (1993–1996). He was chair of the Long Range Planning Committee, URSI. He serves on advisory boards and committees of numerous organizations. He was a Distinguished Microwave Lecturer on Microwave Applications of Metamaterial Structures for the IEEE MTT-S (2004–2006). He was elected a member of the National Academy of Engineering (2003). He was the recipient of a numerous awards including the Shida Award of the Japanese Ministry of Post and Telecommunications (1998), the Japan Microwave Prize (1998), the IEEE Third Millennium Medal (2000), and the IEEE MTT-S Distinguished Educator Award (2000), the Outstanding Career Award from European Microwave Association (2009), the IEEE MTT-S Microwave Career Award (2011), and the Alumni Award for Distinguished Service from the College of Engineering, University of Illinois (2012).